KSCE Journal of Civil Engineering (2018) 22(9):3491-3503

DOI 10.1007/s12205-017-0685-8

Structural Engineering

pISSN 1226-7988, eISSN 1976-3808
www.springer.com/12205

Seismic Behaviors of Steel Bar Reinforced Joints of Concrete Filled Steel Tubular Laminated Columns

Yingying Zhang*, Yuan Huang, Ke Lei***, Jianing Pei****, and Qilin Zhang*****

Received May 28, 2017/Revised October 11, 2017/Accepted October 18, 2017/Published Online December 12, 2017

Abstract

This paper presents the numerical studies on seismic behaviors of steel bar reinforced joints of Concrete Filled Steel Tubular Laminated Columns (CFSTLC). First, the material constitutive relations and modeling details are introduced. Then, the failure mode, bearing capacity and energy dissipation of CFSTLC joints under cyclic loading are studied, in which the effects of concrete grade, steel grade and reinforcement arrangement are discussed. Finally, the restoring force model is proposed to describe the seismic behaviors of bar reinforced joints. Results show that the bar reinforced joints perform good seismic performance. There are three main failure modes, including flexural failure of beam, shear failure of column and mixed failure. Increasing concrete grade and reinforcement ratio of column can increase the ultimate bearing capacity and energy dissipation capacity. Using bundled longitudinal reinforcement bars in beams can slightly reduce the ultimate bearing capacity, but can improve the energy dissipation capacity of specimens with flexural failure modes. Increasing the reinforcement ratio and steel grade can decrease the degradation rate of structural stiffness. The tri-linear restoring force model can make a good prediction of hysteretic behaviors of CFSTLC joints.

Keywords: *Concrete Filled Steel Tubular Laminated Columns (CFSTLC), bar reinforced joints, seismic behaviors, numerical calculation, restoring force model*

1. Introductions

Recently, with development of economy and technology, high-rise buildings are widely welcomed in actual engineering. In high-rise buildings, the load of the bottom columns is always very high, and the "fat beam and big column" phenomenon can be easily observed (Min *et al.*, 2013; Nie, 2011). Therefore, the concept of steel-concrete composite structure is proposed (Ghobarah, 2009; Sakino *et al.*, 2004), which can improve the ductility and seismic performances of heavy-load columns (Fujimoto *et al.*, 2004; Han, 2000).

The concrete filled steel tubular laminated column (abbreviated as CFSTLC), composed of concrete-filled steel tubular column and external reinforced concrete, is first proposed in China (Li *et al.*, 1998). Compared with traditional reinforced concrete columns, the middle steel tube can perform a better ductility (Zhong, 2003). Compared with traditional concrete filled steel tube columns (abbreviated as CFSTC), the outer concrete can effectively reduce the corrosion of steel tube and delay the local buckling of steel tube.

During the construction of CFSTLC, the first step is to pour the inner concrete into the steel tube and then the core column will carry part of vertical load. The second step is to pour the outer concrete and then the load will be re-distributed to the core column and outer concrete. This is the main difference between CFSTLC and CFSTC (Beutel *et al.*, 2002). Due to appearance of steel tube, the mechanical properties of inner and outer concrete both changes. The constraint of steel tube makes the core concrete under a very complex state. The failure of the concrete may change from the original brittle failure to possible plastic failure (Wang *et al.*, 2013). Besides, the steel tube can also improve the strength and ductility of outer reinforced concrete. In addition, the inner and outer concrete may avoid or delay the local buckling of steel tube (CECS, 2005). Then, the stress-strain relation of concrete is very different from the traditional concrete, which is the indispensable basis for the analysis of CFSTLC (Wang, 2011). The ultimate state of CFSTLC subjected to axial compression is the outer concrete achieves the tensile strength,

*Associate Professor, State Key Laboratory for Geomechanics and Deep Underground Engineering, Jiangsu Key Laboratory of Environmental Impact and Structural Safety in Engineering, China University of Mining and Technology, Xuzhou, 221116, China (Corresponding Author, E-mail: zhangyingying85@163.com)
**Master Degree Candidate, State Key Laboratory for Geomechanics and Deep Underground Engineering, Jiangsu Key Laboratory of Environmental Impact and Structural Safety in Engineering, China University of Mining and Technology, Xuzhou, 221116, China (E-mail: hy19910322@163.com)
***Ph.D. China Construction Eighth Engineering Divisions Corp. Ltd, Shanghai, 200135, China (E-mail: leike0307@163.com)
****Master Degree Candidate, State Key Laboratory for Geomechanics and Deep Underground Engineering, Jiangsu Key Laboratory of Environmental Impact and Structural Safety in Engineering, China University of Mining and Technology, Xuzhou, 221116, China (E-mail: 13912034624@qq.com)
*****Professor, College of Civil Engineering, Tongji University, Shanghai, 200092, China (E-mail: qilinzhang0@vip.sina.com)

while the middle of longitudinal reinforcements achieves the compressive strength and the middle stirrups achieve the tensile strength. Additionally, no local buckling of steel tubes is observed, due to the constraint effect of inner and outer concrete (Yao *et al*., 2013). The concrete filled steel tube can improve the shear capacity of core area and simplify the construction. Besides, the outer concrete outside can provide a better fire protection (CECS, 2005).

The experiment method is the most effective method to analyze the mechanical properties of CFSTLC. There have been many experiments on the seismic behaviors of CFSTLC, including axial compression ratio, ultimate load, ductility and energy dissipation. Yao *et al.* (2013) studied on the effects of concrete grade, steel ratio and stirrup characteristic values on the axial compression capacity of CFSTLC and proposed the corresponding design formulas. Wang (2011) studied the eccentric compression of CFSTLC and found that the ultimate state is peripheral compressive damage of outer concrete. When the concrete is crushed, the compression steel bar has achieved the yield strength or very close to the yield strength. The ductility of large eccentric CFSTLC is better than that of small eccentric CFSTLC, but the ultimate bearing capacity decreases with increasing of the eccentricity. Li *et al.* (1999) discussed the failure modes, deformation capacity, energy dissipation and strain distribution of high strength CFSTLC, analyzed the distribution of axial force between concrete and steel tube, and proposed the design formula for the nominal axial compression ratio. Dong *et al.* (2011) found that compared with CFSTC core walls, the CFSTLC core walls can perform better seismic behaviors and the calculations of the simplified model agrees well with the experiment data. Wang (2012) found that using the prestressed steel strips can significantly improve the ductility and seismic performances of high-strength CFSTLC. After the yielding of steel stirrups in outer concrete, the steel strip can serve as a role of "secondary stirrups" and restrain the concrete. Nie (2005) analyzed the effects of outer concrete volume and stirrup ratio on the mechanical properties of columns and deduced the stirrup ratio of outer concrete. Cao *et al.* (2013) studied the seismic behaviors of rectangular CFSTLC with bottom strengthened, and proposed the design formulas.

Recently, due to high calculation efficiency and accuracy, the finite element method has been widely used in the analysis of CFSTLC (Gopal, 2017; Duc, 2013; Tinh, 2016; Duc, 2016a; 2016b). There are a growing number of references on the numerical calculation of CFSTLC (Abbas *et al.*, 2017). Li and Liao built a finite element model to study the mechanical behaviors of CFSTLC subjected to long-term sustained loading, and found that under long-term sustained loading, the ultimate bearing capacity of CFSTRC decreases and the corresponding deflection increases. Hou *et al*. (2014) built a finite element model of CFSTLC under the effects of load and fire and found that under high temperature, the strength of outer concrete decreases and most of the load is carried by steel tube. Li *et al.* (2001) studied the effects of laminate ratio and axial compression ratio on the ultimate strength of CFSTLC, and proposed the design formulas. Xiong (2012) studied the ultimate capacity of CFSTLC high piers, and found that the calculations by using solid elements are inconsistent with the calculations of recommended formulas in design codes. Liao and Han (2010) simulated the cyclic behaviors of CFSTLC, in which the material nonlinearity, bonding-slip between steel bars or steel tube and concrete were considered. Xu *et al.* (2014) studied the effect of preload on the axial bearing capacity of CFSTLC by changing the section size, steel grade and concrete grade and proposed the corresponding design formulas (Evangelista and Brito, 2017).

The current researches are mainly on the seismic performances of CFSTLC, and there are few references on the mechanical properties of beam-column joints. In the construction of bar reinforced joint, when the steel bars pass through the steel tube, the steel tube needs to be slotted. Then, the steel tube after slotted is more prone to fail in the earthquake. Nie *et al.* (2005; 2012) carried out the tests on the seismic behaviors of outer stiffening ring joints, and proposed some constructional methods. Huang and Ling (2001) carried out two CFSTLC joints under cyclic loading and found that with small steel tube and steel plates, the core has excellent energy-dissipation capacity and deformation capacity, although its failure mode is shear failure. Huang. (2008) introduced the design method of related analysis software and constructional proposals of CFSTLC. Zhou *et al.* (2015a; 2015b) studied on the mechanical properties of CFSTLC-ring beams joints by experiment, including failure modes, bearing capacity and energy dissipation, and used ABAQUS to analyze the flexural capacity under different axial force ratio. Besides, for the bar reinforced joint of CFSTLC, the failure mode is not unique. The concrete grade, steel tube grade and reinforcement ratio may affect the failure mode and ultimate bearing capacity of CFSTLC joints. Therefore, it is necessary to study the failure modes and ultimate capacity of bar reinforced joints.

The steel bar reinforced joint is taken as the research object. First, the finite element models are built to simulate the seismic behaviors of bar reinforced CFSTLC joints. Then, the effects of concrete grade, steel tube grade, reinforcement ratio, and reinforcement distribution on the seismic behaviors of CFSTLC joints are studied. Finally, the restoring force model is proposed to describe the seismic behaviors of bar reinforced CFSTLC joints. This paper can provide a good reference for the seismic behaviors of CFSTLC joints.

2. Materials and Methodology

2.1 Constitutive Relation

The finite element method is used to analyze the CFSTLC joints. For steel tube, the perfect elastic-plastic relation is used. For concrete, there are two types of constitutive relations, regarding to the outer and core concrete of CFSTLC.

The stress-strain relation for core concrete in the steel tube is as follows, as shown in Fig. 1 (Han, 2007; Duc, 2017a, 2017b).

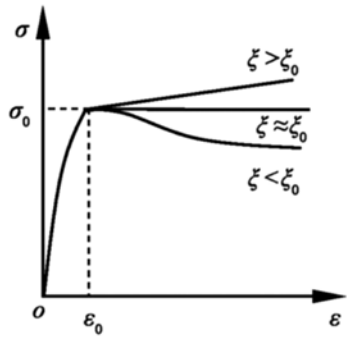

Fig. 1. Stress-strain Relation of Core Concrete

$$y = 2x - x^2 (x \le 1) \tag{1}$$

$$y = \begin{cases} 1+q\cdot(x^{0.1\xi}-1) & (\xi \ge 1.12) \\ \dfrac{x}{\beta\cdot(x-1)^2+x} & (\xi < 1.12) \end{cases} (x>1) \tag{2}$$

where, $x = \dfrac{\varepsilon}{\varepsilon_0}$, $y = \dfrac{\sigma}{\sigma_0}$, ε, σ is the strain and the stress of the concrete, ε_0, σ_0, q, β are the calculation n parameters.

For outer concrete, the damage plastic model is used, according to current design codes (PRC, 2010). The tensile stress-strain relation is as follows.

$$\sigma = (1-d_t)E_c\varepsilon \tag{3}$$

$$d_t = \begin{cases} 1-\rho_t(1.2-0.2x^5) & (x \le 1) \\ 1-\dfrac{\rho_t}{\alpha_t(x-1)^{1.7}+x} & (x>1) \end{cases} \tag{4}$$

$$X = \frac{\varepsilon}{\varepsilon_{t,r}} \tag{5}$$

$$\rho_t = \frac{f_{t,r}}{E_c\varepsilon_{t,r}} \tag{6}$$

Where, α_t is the parameter in the descend phase, $f_{t,r}$ is the uniaxial tensile strength, $\varepsilon_{t,r}$ is the corresponding strain.

The compressive stress-strain relation is as follows.

$$\sigma = (1-d_c)E_c\varepsilon \tag{7}$$

$$d_c = \begin{cases} 1-\dfrac{\rho_c n}{n-1+x^n} & (x \le 1) \\ 1-\dfrac{\rho_c}{\alpha_c(x-1)^2+x} & (x>1) \end{cases} \tag{8}$$

$$\rho_c = \frac{f_{c,r}}{E_c\varepsilon_{c,r}} \tag{9}$$

$$n = \frac{E_c\varepsilon_{c,r}}{E_c\varepsilon_{c,r}-f_{c,r}} \tag{10}$$

$$X = \frac{\varepsilon}{\varepsilon_{c,r}} \tag{11}$$

Where, α_c is the parameter in the descend phase, $f_{c,r}$ is the uniaxial compressive strength, and $\varepsilon_{c,r}$ is the corresponding strain.

2.2 Finite Element Model

The first part is the verification of numerical calculation method by the tests in Qian's reference (Qian and Jiang, 2009). The specimen dimensions and material properties are the same as the tests. Two groups of specimens are named as "CCS1 and CCS2. The compressive strength of concrete in the beam are

Table 1. Details of Test Specimens for Parametric Analysis

Specimen number	Concrete	Steel	Reinforcement solutions	Specimen number	Concrete	Steel	Reinforcement solutions
STRCC1	C40	Q235	With bundle bars	STRCC10	C60	Q345	With bundle bars
STRCC2			No bundle bars	STRCC11			No bundle bars
STRCC3			With bundle bars and increasing reinforcement ratio	STRCC12			With bundle bars and increasing reinforcement ratio
STRCC4		Q345	With bundle bars	STRCC13	C80	Q235	With bundle bars
STRCC5			No bundle bars	STRCC14			No bundle bars
STRCC6			With bundle bars and increasing reinforcement ratio	STRCC15			With bundle bars and increasing reinforcement ratio
STRCC7	C60	Q235	With bundle bars	STRCC16		Q345	With bundle bars
STRCC8			No bundle bars	STRCC17			No bundle bars
STRCC9			With bundle bars and increasing reinforcement ratio	STRCC18			With bundle bars and increasing reinforcement ratio
CCS1	37.9 MPa (beam) 52.5 MPa (in steel tube) 49.3 MPa (out of steel tube)	313 MPa (Yield strength) 391 MPa (ultimate strength)	No bundles bars	CCS2	44.9 MPa (beam) 51.1 MPa (in steel tube) 54.9 MPa (out of steel tube)	313 MPa (Yield strength) 391 MPa (ultimate strength)	No bundles bars

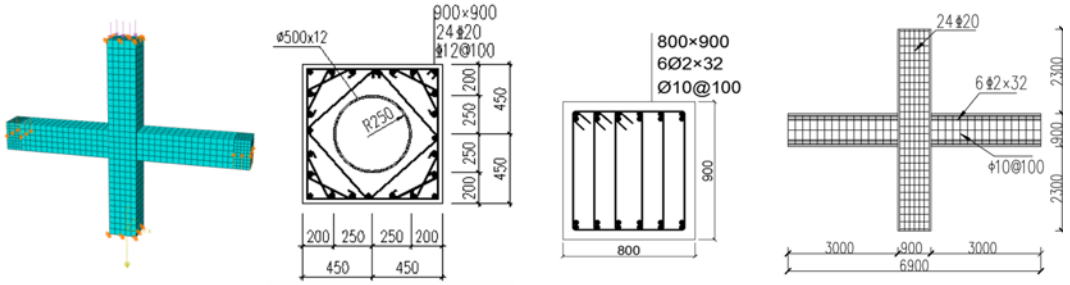

Fig. 2. Dimensions and Finite Element Models of CFSTLC Beam-column Joint (Unit: mm)

37.9 MPa and 44.9 MPa, respectively. The compressive strength of concrete in the steel tube are 52.5 MPa and 51.1 MPa, while those out of the steel tube are 49.3 MPa and 54.9 MPa. For concrete, the elastic modulus and Poisson's ratio is 3.6×10^4 MPa and 0.2. For steel, the elastic modulus and Poisson's ratio is 2.06×10^5 MPa and 0.3. The elements for concrete and steel are C3D8R and C3D8I.

The longitudinal reinforcements and stirrups are HRB400 and HRB 335 and the truss element is used for the reinforcement. The tangent behavior between steel tube and concrete is defined as the penalty contact, and the friction coefficient is 0.3. The normal behavior is defined as the hard contact, in which the steel tube is the main surface and the concrete is the slave surface. The slip effect between steel and concrete is neglected, and the embedded contact is conducted (Nie *et al*., 2012). The column ends are fixed by hinge joint. The axial force is applied in all the components of the column top and the axial compression ratio is 0.3. The loading protocol is controlled by displacement, every increment is 10 mm and two cycles in one level. Besides, the gasket that is defined as the rigid body is applied in the column top, in order to avoid the local crushing of concrete.

The second part is the parametric analysis on bar reinforced joints of CFSTLC. There are 18 specimens and the details are shown in Fig. 2 and Table 1. It should be noticed that the parameters for CCS1 and CCS2 are the measured values of joint experiments. All the specimens have the same dimension. The column is with the cross section of 900 mm × 900 mm and the height of 5.5 m. The beam is with the cross section of 800 mm × 900 mm and the length of 6m. The steel tube is with the outer diameter of 512 mm and the thickness of 12 mm. All the reinforcements are HRB400 and all the stirrups are HPB300. For the column, the longitudinal reinforcement of column is 24ϕ20 and the stirrup is ϕ12@100. For the beam, the upper and bottom reinforcements are 6ϕ2 × 32, and the stirrup is ϕ10@100.

The mass density of concrete is 2.4×10^3 kg/m^3, and the elastic modulus are 3.25×10^4 MPa (C40), 3.6×10^4 MPa (C60), and 3.8×10^4 MPa (C80), respectively. The boundary conditions are the same as the referenced tests. The steel gaskets are set in the column ends and the hinge conditions are used. The loading protocol is controlled by displacement.

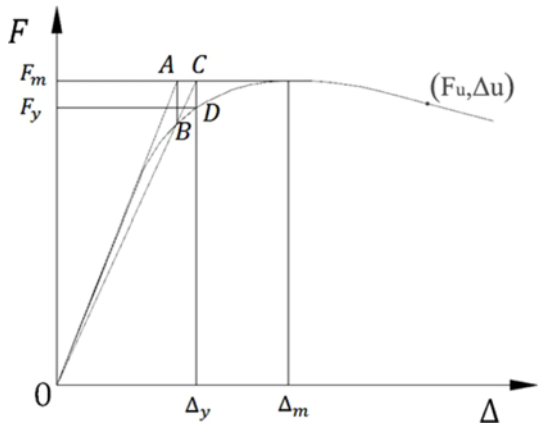

Fig. 3. Determination of Yield Point and Ultimate Point

3. Results and Discussions

3.1 Verification of Numerical Calculation Method

Table 2 shows the comparisons between numerical calculations and experiment data in Qian's reference (Qian and Jiang, 2009). Where, F_y, Δ_y, θ_y are the yielding load, displacement and rotation angle. The yielding points can be determined as shown in Fig. 3. Where, F_m, Δ_m, θ_m are the peak load, displacement and rotation angle, and F_u, Δ_u, θ_u are the failure load, displacement and rotation angle. It can be observed that the peak load of the numerical calculation is about 10% higher than the experiment data. This is because in the experiment, the concrete strength may not achieve the design strength, due to lack of enough vibration in the concrete pouring. As shown in Fig. 4, the lateral load-lateral displacement hysteretic curve of column in the numerical calculation seems better than the test curves. Besides, ignoring of bar slip may also lead to the slight differences between experiment data and numerical calculation (Wang *et al.*, 2013).

The skeleton curves of three specimens are shown in Fig. 5. It can be seen that for yielding displacement and peak displacement, the numerical value is consistent with the experiment data. The skeleton curves of CCS1 and CCS2 descend significantly after the peak point. This is mainly because that after the cracking of outer concrete, the reinforcement yields fast because of ignoring the slip between bar and concrete (Wang *et al*., 2013) . After the appearance of concrete crack, the bar stress increases fast and it

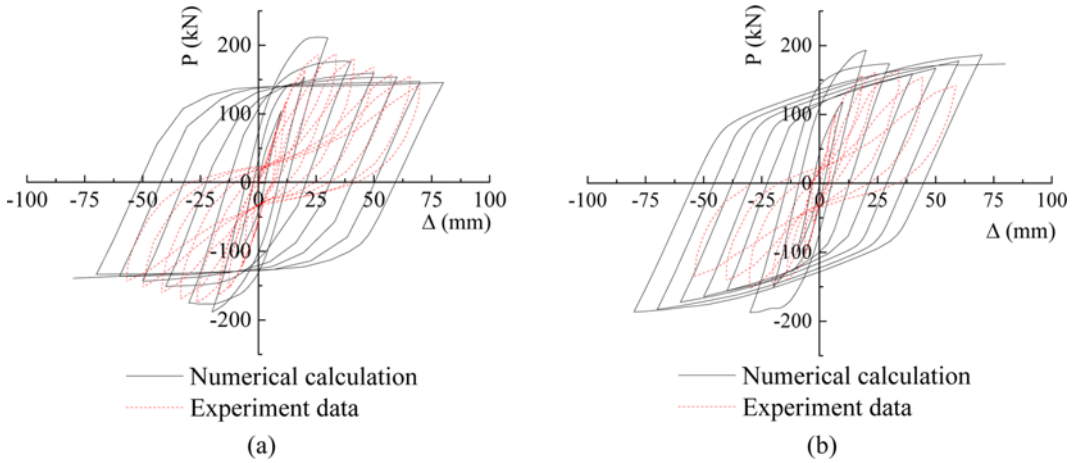

Fig. 4. P-Δ Hysteresis Curves of Specimens: (a) CCS1, (b) CCS2

Table 2. Comparisons between the Numerical Simulation and Experiment Data of CFSTLC

Specimen		CCS1			CCS2		
		Numerical calculation	Experiment data	Difference	Numerical calculation	Experiment data	Difference
Yielding	F_y (kN)	170	170	0%	153	154	0.6%
	Δ_y (mm)	22	19	13.6%	15	18	16.7%
	θ_y	1/64	1/71	9.8%	1/93	1/77	17.2%
Peak	F_m (kN)	210	187	10.9%	193	166	16.2%
	Δ_m (mm)	30	33	10.0%	25	36	30.5%
	θ_m	1/47	1/43	9.3%	1/56	1/39	30.3%
Final	F_u (kN)	178	144	19.0%	164	143	12.8%
	Δ_u (mm)	42	70	40.0%	40	60	33.3%
	θ_u	1/33	1/20	34.0%	1/35	`1/23	34.2%

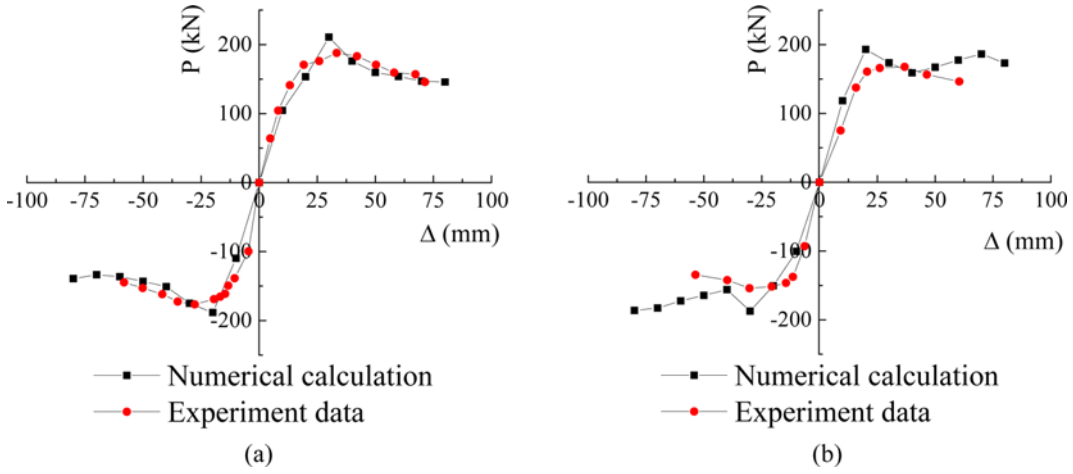

Fig. 5. Skeleton Curves of Specimens: (a) CCS1, (b) CCS2

is easy to achieve the yielding points. Meanwhile, the displacement in the numerical calculation is always lower than the measured displacement. This is also why the degradation of skeleton curve is so significant in the numerical calculation.

The failure stress of joints are show in Fig. 6. For CCS1 and CCS2, the failure modes are shear failure in the core area. In the core area, the maximum stress of concrete appears along the diagonal line. For the outer concrete, the crack also appears along the diagonal line. Most of steel tube and stirrup yields, while the shear force is carried by outer concrete, stirrup and steel tube. For CCS2, the stress of outer concrete is higher than CCS1. From the hysteretic curves and skeleton curves, increasing the stirrup can improve the energy dissipation ability. The numerical calculation is consistent with the experiment data. The analysis

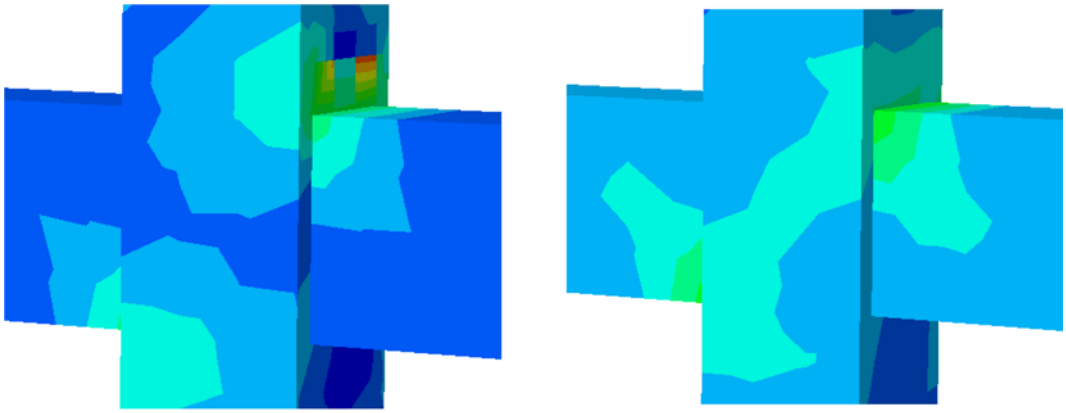

Fig. 6. Failure Modes of Specimens: (a) CCS1, (b) CCS2

Table 3. Numerical simulations of CFSTLC

Specimen number	Concrete	Steel	Yield			Peak			Failure		
			F_y (kN)	Δ_y (mm)	θ_y	F_m (kN)	Δ_m (mm)	θ_m	F_u (kN)	Δ_u (mm)	θ_u
STRCC1	C40	Q235	697	6	1/500	848	16	1/188	721	39	1/77
STRCC2			698	6	1/500	850	16	1/188	723	38	1/79
STRCC3			1311	8	1/375	1506	20	1/150	1400	40	1/75
STRCC4		Q345	683	8	1/375	840	16	1/188	714	38	1/79
STRCC5			542	8	1/375	663	14	1/214	564	40	1/75
STRCC6			1045	8	1/375	1257	18	1/167	1068	38	1/79
STRCC7	C60	Q235	779	6	1/500	1060	20	1/150	1058	40	1/75
STRCC8			663	6	1/500	907	16	1/188	969	40	1/75
STRCC9			1254	8	1/375	1539	20	1/150	1499	40	1/75
STRCC10		Q345	779	6	1/500	1060	16	1/188	1086	40	1/75
STRCC11			880	6	1/500	1220	16	1/188	1219	40	1/75
STRCC12			1332	6	1/500	1542	18	1/167	1402	40	1/75
STRCC13	C80	Q235	798	6	1/500	1080	16	1/188	918	39	1/77
STRCC14			877	6	1/500	1168	16	1/188	993	38	1/79
STRCC15			1667	8	1/375	2000	18	1/167	1700	36	1/83
STRCC16		Q345	1023	8	1/375	1234	18	1/167	1049	39	1/77
STRCC17			1054	8	1/375	1259	18	1/167	1070	39	1/77
STRCC18			542	6	1/500	660	14	1/214	561	40	1/75

method of numerical calculation can be used to simulate the seismic behaviors of beam-column joints of CFSTLC.

3.2 Numerical Simulation of Bar Reinforced Joint of CFSTLC

This part mainly presents the hysteretic behaviors of bar reinforced joint of CFSTLC under cyclic loading. The numerical calculation results of bar reinforced joint of CFSTLC are shown in Table 3.

For the specimens (STRCC1~STRCC3), when the concrete of beam is C40 and the steel tube is Q235, changing the reinforcement distribution has little effects on the peak load, but increasing the reinforcement ratio can enhance the peak load. For the specimens (STRCC4 ~ STRCC9), when the concrete is C40 and the steel tube is Q345, or the concrete is C60 and the steel tube is Q235, using the bundled bars can lower the peak load, while increasing the reinforcement ratio can enhance the peak load. For the specimens (STRCC10 ~ STRCC18), when the concrete is C60 or C80 and the steel tube is Q345, using the bundled bars can decrease the peak load, while increasing the reinforcement ratio can enhance the peak load.

For the specimens (STRCC1, STRCC4, STRCC7, STRCC10, STRCC13 and STRCC16), when the concrete is C80, increasing the grade of steel tube or beam concrete can enhance the peak load. However, when the concrete is C40 or C60, the effect of steel grade is not significant. When the steel grade is Q235, when the concrete is higher than C60, increasing of concrete grade has no effects on the peak loads.

3.3 Failure Modes

Figure 7 shows the failure modes and stress distributions of bar

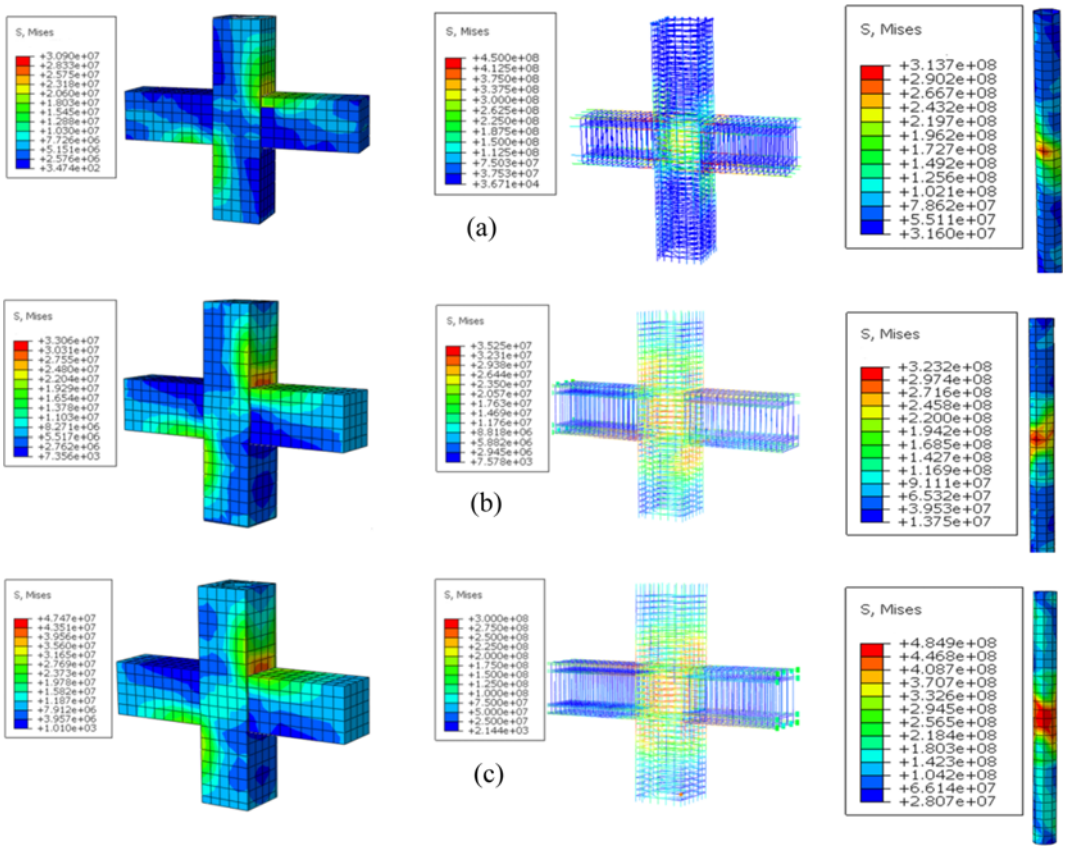

Fig. 7. Failure Modes and Stress Distribution of Bar Reinforcement Specimens: (a) Flexural Failure of Beam, (b) Mixture Failure, (c) Shear Failure of Column

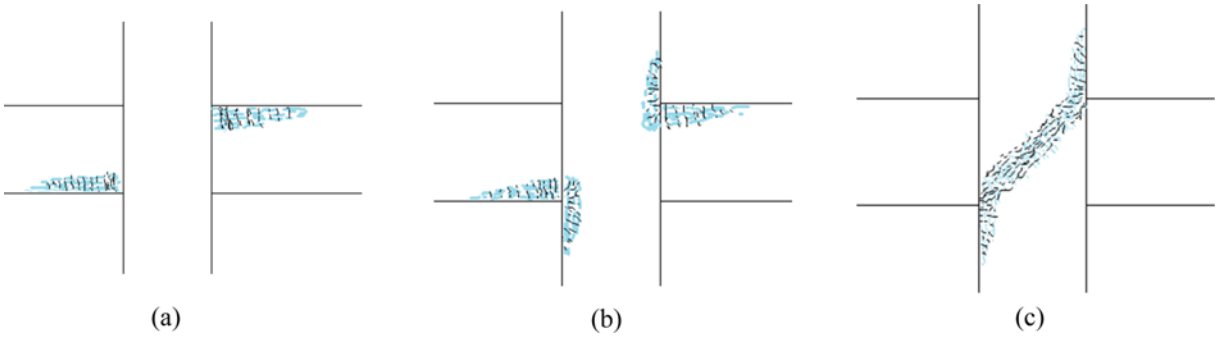

Fig. 8. Principal Plastic Strain Vectors of Concrete: (a) Flexural Failure of Beam, (b) Mixture Failure, (c) Shear Failure of Column

reinforced specimens. Fig. 8 shows the principle plastic strain vectors of concrete. The appearance of principal tensile plastic strain means the cracking of concrete and the orientation of crack is perpendicular to the principal tensile plastic strain (Lee and Fenves, 1998; Hong, 2017).

There are three main failure modes, including flexural failure of beam, shear failure of column and mixed failure. First, as shown in Fig. 7(a), the failure mode is flexural failure of beam. This type of failure mode always appears when the concrete strength of beam or the reinforcement ratio of beam is low. Then, the loading capacities of column and core area are relatively higher, compared with the beam. Therefore, the failure first appears in the concrete in the compressive area of beam end. After the concrete is crushed, the reinforcement bars in the compressive area yield. Then, the concrete, steel tube and reinforcement bars in the core area of column does not achieve the yield strength. Second, as shown in Fig. 7(c), the failure mode is shear failure of column. This type of failure mode always appears because when the concrete strength of column or the ratio of stirrups of column is low. Then, the shear force is mainly carried by the outer concrete of the core area, but the column can not afford enough shear resistance. Therefore. the diagonal crack first appears in the outer of the core area of column. When the load increases, the stress of outer concrete

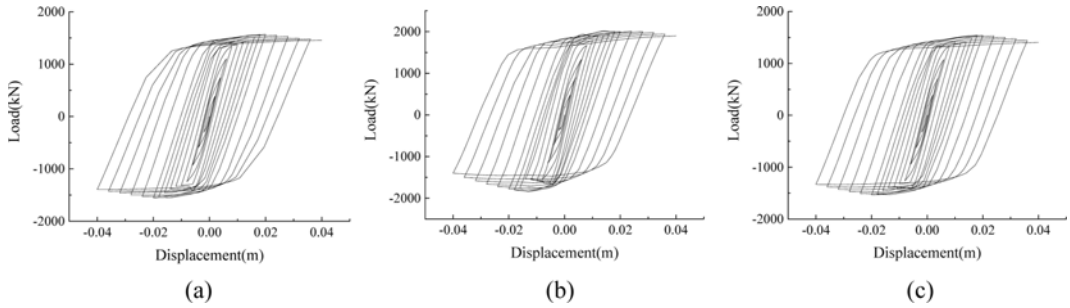

Fig. 9. Hysteresis Curves of Bar Reinforced Specimens: (a) STRCC6, (b) STRCC15, (c) STRCC12

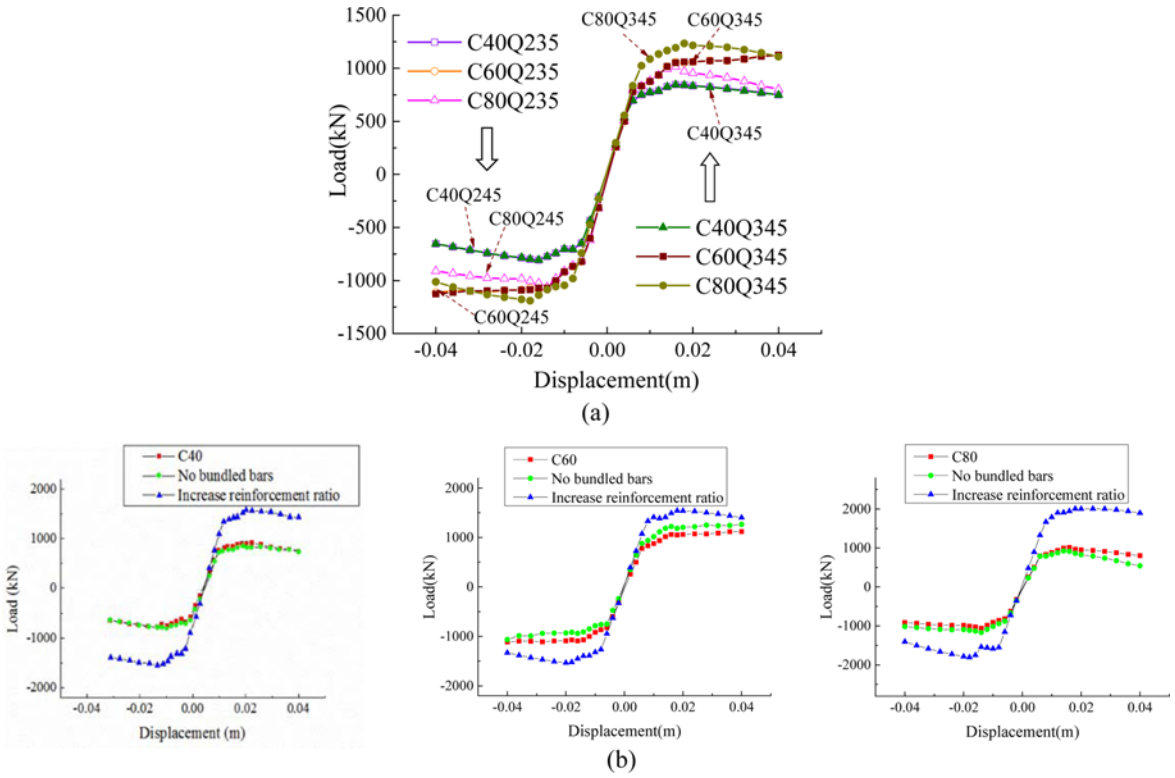

Fig. 10. Skeleton Curves of Bar Reinforced Specimens: (a) Effect of Concrete Grade and Steel Grade (with no reinforcement solutions), (b) Effect of Bar Distribution and Reinforcement Ratio

increase, and the shear force is mainly carried by concrete, steel tube and stirrup. When the specimen fail, the outer concrete is crushed along the diagonal line, while the steel tube and stirrups yield together. Third, as shown in Fig. 7(b), the failure mode is mixed failure of shear failure and flexural failure. This type of failure mode appears when the concrete strength is intermediate, Then, the loading capacity of beam is close to that of the column. When the specimens fail, the reinforcement bars in the compressive zone and stirrups in the column yield, while the concrete in the compressive zone is crushed. Then, the diagonal crack mainly appears in the connection of beam and column.

3.4 Hysteretic Curves and Skeleton Curves

The hysteretic curves and skeleton curves are shown in Fig. 9 and Fig. 10. It can be seen that the load-displacement curves perform good energy dissipation ability and ductility (Nie *et al.*, 2012; Duc *et al.*, 2017). There are four phases in the skeleton curves, including elastic, elastic-plastic, plastic and failure. It is a typical ductile failure mode.

The concrete grade, steel grade and reinforcement ratio have obvious effects on the ultimate loading capacity of bar reinforced joints. When the steel grade is high, increasing concrete grade can enhance the ultimate loading capacity of specimens under reversed cyclic loading. The peak loads increase about 20%, when the concrete grades increase 20%. When the steel grade is low, increasing the concrete grade can enhance the ultimate bearing capacity. This is because decreasing of steel grade may lead to the shear failure of column cores. When the concrete is C60, the failure mode is shear failure of columns. Then, increasing the concrete grade has little effects on the ultimate capacity of specimens. According to the seismic requirements, the shear failure of columns should be avoided in the design and

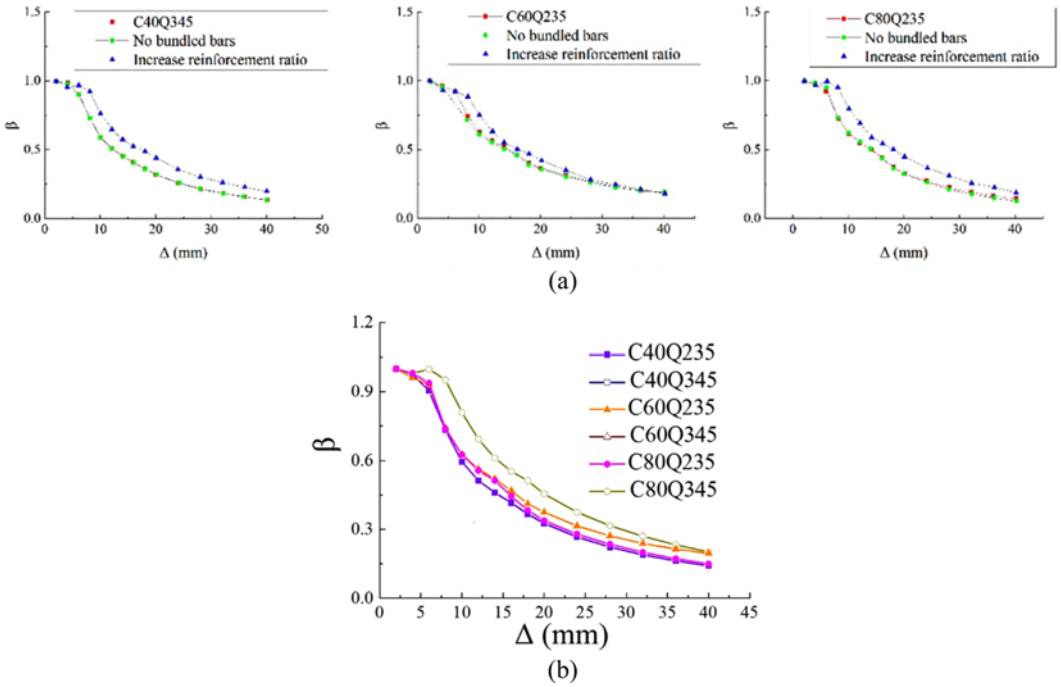

Fig. 11. Stiffness Degradations of Bar Reinforced Specimens: (a) Effect of Bar Distribution and Reinforment, (b) Effect of Concrete Grade and Steel Grade (with no reinforement solutions)

analysis of CFSTLC.

Figure 10(a) shows that when the concrete is C40 or C60, increasing the grade of steel tube has little effects on the ultimate loading capacity. When the concrete is C80, increasing the grade of steel tube can enhance the ultimate loading capacity. When the concrete grade increases, the failure mode changes from "flexural failure of beam to "shear failure of column. Then, increasing the grade of steel tube can enhance the shear capacity of columns.

Figure 10(b) show using bundle bars leads to the slight decrease of ultimate bearing capacity of bar reinforced specimens, less than 10%. The equivalent diameter is about 1.41 times of a single bar (PRC, 2010). From above, using bundle bars can increase the ultimate capacity and energy dissipation energy. Additionally, it can avoid using smaller bar diameter and dense distribution of stirrups.

3.5 Stiffness Degradation

In order to study the stiffness degradations, the secant stiffness of specimens under cyclic loading can be calculated (Clough, 1966). Fig. 11 shows the degradation curves of specimens. Where, β is the ratio of secant stiffness K_i and initial stiffness K_1 (Tang, 1989).

As shown in Fig. 11, significant stiffness degradation can be observed. In the initial, the structural stiffness decreases slowly, and the degradation rate increases after the yielding points. Fig. 11(a) shows that increasing the reinforcement ratio can decrease the degradation ratio of specimen stiffness, while the changing of reinforcement distribution has little effects on the degradation of specimen stiffness. Fig. 11(b) shows when the grade of steel tube is lower, changing the concrete grade has no effects on the degradation of specimen stiffness. However, when the grade of steel tube is high, increasing the concrete grade can decrease the degradation ratio of structural stiffness. Fig. 11(b) shows when the concrete is C80, increasing the steel grade can decrease the degradation ratio of structural stiffness. When the concrete is C40 and C60, changing the grade of steel tube can slightly increase the degradation ratio of specimen stiffness.

3.6 Energy Dissipation Analysis

Figure 12 shows the accumulative energy dissipation curves of bar reinforced specimens under reversed cyclic loading. From Fig. 12(a), for the specimens whose failure mode is flexural failure of beam, using the bundled bars can enhance the energy dissipation ability of specimens. For the specimens whose failure mode is shear failure of column, using bundled bars has no effects on the energy dissipation ability of specimens. For all the specimens, increasing the reinforcement ratio can enhance the energy dissipation ability of specimens. From Fig. 12(b), when the concrete change from C40 to C60, the total energy dissipation increases about 25%. However, when the concrete changes from C60 to C80, the total energy dissipation remains almost unchanged. Then, the failure modes of bar reinforced specimens change from "flexural failure of beam to "shear failure of column. From Fig. 12(b), changing the grade of steel tube has little effects on the accumulative energy dissipation.

3.7 Restoring Force Model

The tri-linear restoring force model is conducted to describe the restoring force characteristics of bar reinforced joints of CFSTLC, as shown in Fig. 13. It can consider the stiffness

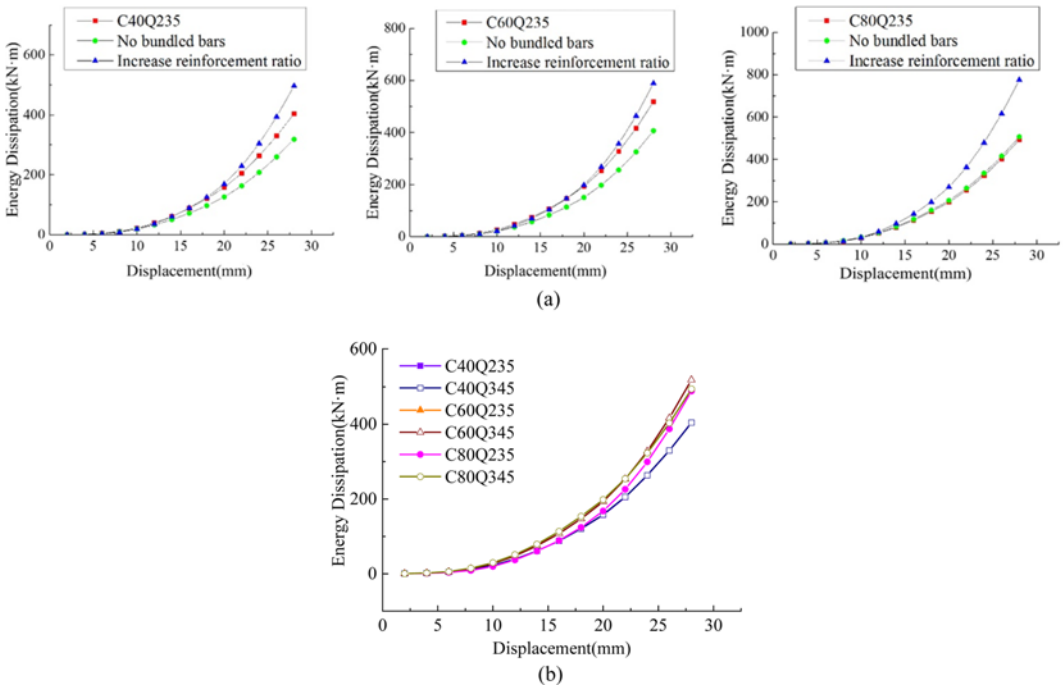

Fig. 12. Accumulative Energy Dissipation Curves of Bar Reinforced Specimens: (a) Effect of Bar Distribution and Reinforcement Ratio, (b) Effect of Concrete Grade and Steel Grade (no reinforcement solutions)

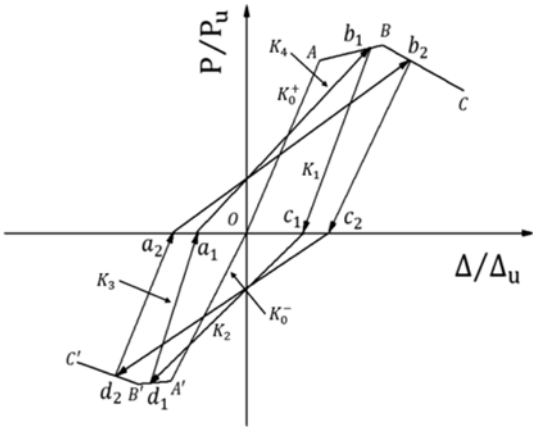

Fig. 13. Tri-linear Model Considering Stiffness Degradation

degradation and is suitable for the seismic analysis of the CFSTLC. The dimensionless method is used to reduce the effect of experimental parameters on the restoring force model. Where, the vertical ordinate is the ratio of the load P to the peak load P_u, The horizontal ordinate is the ratio of displacement Δ to peak displacement Δ_u. A and A' are the yield points, B and B' are the peak points, C and C' are the ultimate points.

All the dimensionless skeleton curves were analyzed by regression analysis, as shown in Fig. 14. All the segments can be obtained by the data in Fig. 14. The regression equation for each segment is shown in Eq. (12).

$$P/P_u = k \cdot \Delta/\Delta_u + b \tag{12}$$

From the numerical calculations, the stiffness degradation can be observed for the bar reinforced CFSTLC joints under low cyclic loading. In order to study the restoring force model, the degradation law of loading stiffness and unloading stiffness of joints under low cyclic loading can be obtained first. Where, K_0 is the initial stiffness of the specimen, K_1 is the forward unloading stiffness, K_2 is the reverse loading stiffness, K_3 is the reverse unloading stiffness and K_4 is the forward loading stiffness.

The degradation of forward unloading stiffness K_1 can be described as:

$$K_1/K_0^+ = -0.1\ln(\Delta_1/\Delta_0^+) + 0.689 \tag{13}$$

The degradation of reverse loading stiffness K_2 can be expressed as:

$$K_2/K_0^- = 0.973e^{-0.729(\Delta_1'/\Delta_0^+)} \tag{14}$$

The degradation of reverse unloading stiffness K_3 can be expressed as:

$$K_3/K_0^- = -0.118\ln(\Delta_2/\Delta_0^-) + 0.741 \tag{15}$$

The degradation of forward loading stiffness K_4 can be expressed as:

$$K_4/K_0^+ = 0.822e^{-0.644(\Delta_2'/\Delta_0^-)} \tag{16}$$

Figure 15 shows the comparisons between the predictions of restoring force models and numerical calculations. The restoring force model can make a good prediction of yielding points, peak points, ultimate points and load-displacement curves. The simplified tri-linear curves agree well with the numerical skeleton curves.

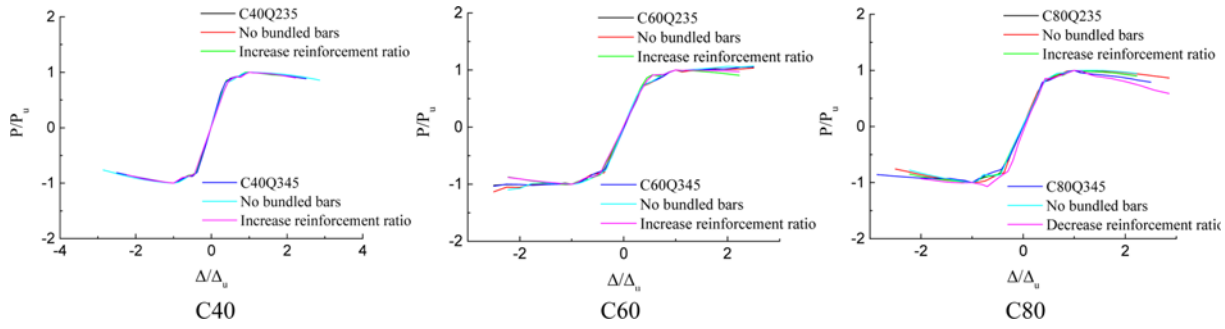

Fig. 14. Non-dimensional Skeleton Curves of Bar Reinforced Joint

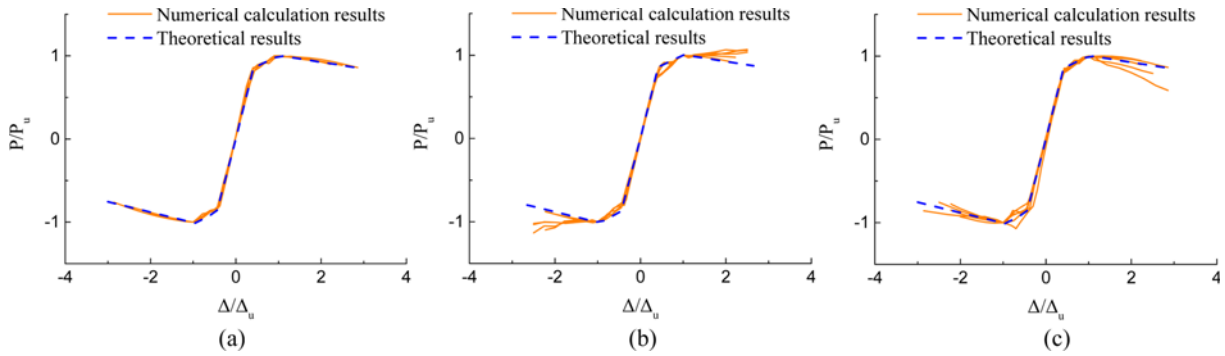

Fig. 15. Comparisons between Model Predictions and Numerical Simulations for Bar Reinforced Joints: (a) C40, (b) C60, (c) C80

In Fig. 15(b), the numerical simulation results are slightly higher than the theoretical results. This is because that the failure mode of these specimens are mixture failure of shear failure and flexural failure, and there are two diagonal cracks in the core area of the column. However, these cracks did not continue to develop with the increase of load, the stiffness of the specimen was not significantly degraded after yielding. From above, the proposed restoring force model for the CFSTLC specimens is reliable and can be used for the seismic analysis.

4. Conclusions

This paper presents the numerical calculation on the seismic behaviors of bar reinforced CFSTLC joints and proposed the restoring force model. The following conclusions can be obtained.

1. There are three types of failure modes of bar reinforced joints, including flexural failure of beam, shear failure of column and mixture failure of shear and flexural. When the grade of beam concrete and the reinforcement ratio is low, the failure mode is flexural failure of beam. Then, the failure occurs in the concrete of beam end, while the longitudinal reinforcements yield. When the grade of beam concrete is high but the steel tube strength is low, the failure mode is shear failure of column. The outer concrete, stirrups, and steel tube achieve the yielding stress and the failure mode is the shear damage of column core area. When the concrete strength, reinforcement ratio, and strength of steel tube is intermediate, the damage happens at the beam-column joints, which is mixed failure of shear and flexural. Then, the concrete in beam end is crushed and the outer concrete of core area is shear failure, while part of the longitudinal reinforcement and column stirrups yields.
2. For bar reinforced CFSTLC joints, increasing the concrete grade of beam can increase the ultimate capacity and energy dissipation capacity of specimens with flexural failure modes. Increasing the ratio of longitudinal reinforcements can improve the energy dissipation ability of all specimens, but only improve the ultimate capacity of specimens with flexural failure modes. Using bundled bars can slightly reduce the bearing capacity of specimens, but can greatly increase the energy dissipation capacity of specimens. Increasing the grade of steel tube can effectively improve the shear capacity of CFSTLC, but has no effects on the energy dissipation capacity.
3. The dimensionless method is used to reduce the effect of concrete strength and steel strength on the restoring force characteristics of joints. The tri-linear restoring force model of bar reinforced CFSTLC joints can be obtained based on the skeleton curves. The predictions of the restoring force model agree well with the numerical simulations. It can provide good references for the seismic analysis of similar joints.

Acknowledgements

This work is supported by the Fundamental Research Funds

for the Central Universities under (Grant No. 2015QNA57). The authors acknowledge the editors and reviewers for their valuable comments on an earlier draft of this paper.

References

Abbas, H., Al-Salloum, Y., Alsayed, S., Alhaddad, M., and Iqbal, R. (2017). "Post-heating response of concrete-filled circular steel columns." *KSCE Journal of Civil Engineering*, Vol. 21, No. 4, pp. 1367-1378, DOI: 10.1007/s12205-016-0852-3.

Beutel, J., Thambiratnam, D., and Perera, N. (2002). "Cyclic behaviour of concrete filled steel tubular column to steel beam connections." *Engineering Structures*, Vol. 24, No. 1, pp. 29-38, DOI: 10.1016/S0141-0296(01)00083-9.

Cao, W., Hui, C., Dong, H., Fangfang, X. U., and Qiao, Q. (2013). "Study on seismic behavior of bottom strengthened rectangular steel tube reinforced concrete columns." *World Earthquake Engineering*, Vol. 29, No. 3, pp. 14-19, DOI: 1007-6069 (2013) 03-0014-06.

China Engineering Construction Standardization Association (2005). *CECS188:2005*, Technical specification for steel tube-reinforced concrete column structure, Tsinghua University; Beijing, China.

Clough, R. W. (1966). *Effect of stiffness degradation on earthquake ductility requirements*, Ph.D. Thesis, Univ. of California, California, United States of America.

Dong, H. Y., Geng, H. X., Zhang, J. W., Cao, W. L., and Yang, X. Q. (2011). "Experimental study on seismic behavior of composite core walls with steel tube-reinforced concrete columns." *Journal of Beijing University of Technology*, Vol. 37, No. 11, pp. 1720-1728, DOI: 0254-0037(2011)11-1720-09.

Duc, N. D. (2013). "Nonlinear dynamic response of imperfect eccentrically stiffened FGM double curved shallow shells on elastic foundation." *Composite Structures*, Vol. 99, pp. 88-96, DOI: 10.1016/j.compstruct.2012.11.017.

Duc, N. D. (2016a). "Nonlinear thermal dynamic analysis of eccentrically stiffened S-FGM circular cylindrical shells surrounded on elastic foundations using the Reddy's third-order shear deformation shell theory." *European Journal of Mechanics* - A/Solids, Vol. 58, pp. 10-30, DOI: 10.1016/j.euromechsol.2016.01.004.

Duc, N. D. (2016b). "Nonlinear thermo-electro-mechanical dynamic response of shear deformable piezoelectric Sigmoid functionally graded sandwich circular cylindrical shells on elastic foundations." *Journal of Sandwich Structures and Materials*, first published online: June 8, 2016, DOI: 10.1177/1099636216653266.

Duc, N. D., Kim, S.-E., Cong, P. H., Anh, N. T., and Khoa, N. D. (2017). "Dynamic response and vibration of composite double curved shallow shells with negative Poisson's ratio in auxetic honeycombs core layer on elastic foundations subjected to blast and damping loads." *International Journal of Mechanical of Sciences*, Vol. 133, pp. 504-512, DOI: 10.1016/j.ijmecsci.2017.09.009.

Duc, N. D., Kim, S. E., Tuan, N. D., Phuong Tran, and Khoa, N. D. (2017). "New approach to study nonlinear dynamic response and vibration of sandwich composite cylindrical panels with auxetic honeycomb core layer." *Journal Aerospace Science and Technology*, 2017, Vol. 70, pp. 396-404, DOI: 10.1016/j.ast.2017.08.023.

Evangelista, L. and Brito, J. D. (2017). "Flexural behaviour of reinforced concrete beams made with fine recycled concrete aggregates." *KSCE Journal of Civil Engineering*, Vol. 21, No. 1, pp. 353-363, DOI: 10.1007/s12205-016-0653-8.

Fujimoto, T., Mukai, A., Nishiyama, I., and Sakino, K. (2004). "Behavior of eccentrically loaded concrete-filled steel tubular columns." *Journal of Structural Engineering*, Vol. 130, No. 2, pp. 203-212, DOI: 10.1061/(ASCE)0733-9445(2004)130:2(203).

Ghobarah, A. (2009). "Performance-based design in earthquake engineering: State of development." *Engineering Structures*, Vol. 23, No. 8, pp. 878-884, DOI: 10.1016/S0141-0296(01)00036-0.

Gopal, S. R. (2017). "An experimental study on FRC infilled steel tubular columns under eccentric loading." *KSCE Journal of Civil Engineering*, Vol. 21, No. 3, pp. 923-927, DOI: 10.1007/s12205-016-0851-4.

Han, L. H. (2000). *Concrete-Filled Steel Tube Structure*, Science Press, Beijing, China.

Han, L. H. (2007). *Concrete-Filled Steel Tube Structure—Theory and Practice 2nd Ed*, Science Press, Beijing, China.

Hong, D. N., Tinh, B. Q., Thom, V. D., and Duc, N. D. (2017). "A rate-dependent hybrid phase field model for dynamic crack propagation." *Journal of Applied Physics*, Vol. 122, No. 11, 115102, DOI: 10.1063/1.4990073.

Hou, S. L., Han, L. H., and Song, T. Y. (2014). "Analysis on concrete-encased CFST columns under fire." *Engineering Mechanics*, Vol. 31, No. Suppl, pp. 109-114, DOI: 1000-4750(2014)Suppl-0109-06.

Huang, Y. (2008). "Design and calculation of steel tube-reinforced concrete column." *Steel Construction*, Vol. 23, No. 7, pp. 12-19, DOI: 10.3969/j.issn.1007-9963.2008.07.004.

Huang, Z. and Ling, L. (2001). "Experimental study and finite element analysis on shear behavior of steel tube fill high strength concrete composite column core area." *Industrial Construction*, Vol. 31, No. 7, pp. 50-53, DOI: 10.13204/j.gyjz2001.07.018.

Lee, J. and Fenves, G. L. (1998). "Plastic-damage model for cyclic loading of concrete structures."*Journal of Engineering Mechanics*, Vol. 124, No. 8, pp. 892-900, DOI: 10.1061/(ASCE)0733-9399(1998)124:8(892).

Li, H., Wu, B., and Lin, L. Y. (1998). "Study on seismic properties of laminated column with high strength concrete containing steel tube." *Earthquake Engineering & Engineering Vibration*, Vol. 18, No. 1, pp. 45-53, DOI: 10.13197/j.eeev.1998.01.007.

Li, H., Liu, K. M., Wu, B., and Zhang, P. (2001). "Calculation for ultimate strength of steel encased high-strength concrete laminated columns." *Journal of Harbin University of Civil Engineering & Architecture*, Vol. 34, No. 3, pp. 1-4, DOI: 1006-6780(2001)03-0001-04.

Li, Y. J. and Liao, F. Y. (2013). "Behaviour of concrete filled steel tube reinforced concrete columns subjected to long-term sustained loading." *Journal of Beijing University of Technology*, Vol. 39, No. 8, pp. 1187-1191, DOI: 0254-0037 (2013)08-1187-06.

Liao, F. Y. and Han, L. H. (2010). "Performance of concrete-filled steel tube reinforced concrete columns with square sections." *Engineering Mechanics*, Vol. 27, No. 4, pp. 153-162, DOI: 1000-4750(2010)04-0153-10.

Min, Y. U., Zha, X., Jianqiao, Y. E., and Yuting, L. I. (2013). "A unified formulation for circle and polygon concrete-filled steel tube columns under axial compression." *Engineering Structures*, Vol. 49, No. 2, pp. 1-10, DOI: 10.1016/j.engstruct.2012.10.018.

Nie, J. G., Wang, Y. H., and Fan, J. S. (2012). "Experimental study on seismic behavior of concrete filled steel tube columns under pure torsion and compression–torsion cyclic load." *Journal of Constructional Steel Research*, Vol. 79, No. 1, pp. 115-126, DOI: 10.1016/j.jcsr.2012.07.029.

Nie, J. G. (2005). "Analyses on composite column with inside concrete filled steel tube under axial compression." *China Civil Engineering*

Journal, Vol. 38, No. 9, pp. 9-13, DOI: 10.15951/j.tmgcxb.2005.09.002.

Nie, J. G. (2011). *Steel-Concrete Combination Structure*, China Architecture &Building Press, Beijing, China.

Nie, J., Jie, Z., Yu, B., and Yan, X. (2005), "Bearing capacity of axially compressed core columns having concrete-filled steel tubes." *Journal of Tsinghua University*, Vol. 45, No. 9, pp. 1153-1156, DOI: 10.16511/j.cnki.qhdxxb.2005.09.001.

Nie, J. G., Wang, Y. H., Tao, M. X., and Tan, W. (2012). "Experimental study on seismic behavior of laminated steel tube column-concrete beam joint with outer stiffening ring." *Journal of Building Structures*, Vol. 33, No. 7, pp. 88-97, DOI: 10.14006/j.jzjgxb.2012.07.011.

PRC, M. O. C. (2003). *GB50017-2003*, Code for design of steel structures, MOHURD; Beijing, China.

PRC, M. O. C. (2015). *JGJ/T 101-2015*, Specification for seismic test of building, MOHURD; Beijing, China.

PRC, M. O. C. (2010). *GB50010-2010*, Code for design of concrete structures, MOHURD; Beijing, China.

Qian, J. R. and Jiang, Y. (2009). "Tests on seismic behavior of RC beam-composite steel tube confined concrete column joints." *Building Structure*, Vol. 39, No. 9, pp. 39-42 (don´t have DOI).

Sakino, K., Nakahara, H., Morino, S., and Nishiyama, I. (2004). "Behavior of centrally loaded concrete-filled steel-tube short columns." *Journal of Structural Engineering*, Vol. 130, No. 2, pp. 180-188, DOI: 10.1061/(ASCE)0733-9445(2004)130:2(180).

Tang, J. R. (1989). *Seismic Analysis For Joints of Reinforced Concrete Frame*, Southeast University Press, Nanjing, Jiangsu, China.

Tinh, Q. B., Duc, H. D., Thom, V. D., Sohichi Hirose, and Duc, N. D. (2016). "High frequency modes mesh free analysis of Reissner-Mindlin plates." *Journal of Science: Advanced Materials and Devices*, Vol. 3, No. 1, pp. 400-412, DOI: 10.1016/j.jsamd.2016.08.005.

Varma, A. H., Ricles, J. M., Sause, R., and Lu, L. W. (2002). "Seismic behavior and modeling of high-strength composite Concrete-filled Steel Tube (CFT) beam-columns." *Journal of Constructional Steel Research*, Vol. 58, Nos. 5-8, pp. 725-1758, DOI: 10.1016/S0143-974X(01)00099-2.

Wang, B. (2011), *Research on eccentric compression experiment and load-bearing capacity calculation of steel tube-reinforced concrete colum*n, M.S. Thesis, Taiyuan University of Technology, Taiyuan, Shanxi, China.

Wang, Q., Zhu, L. L., Li, Z., Wang, Z., and Liu, L. (2013). "Study on the constitutive model of steel for explicit dynamic beam elements of ABAQUS." *China Journal of Civil Engineering*, Vol. 46, No. Supp2, pp. 100-105, DOI: 10.15951/j.tmgcxb.2013.s2.027.

Wang, W., Li, W. Q., and Chen, Y. (2013). "Experimental study on seismic behavior of concrete filled steel tubular column-to-RC ring beam joints in three dimensional frames." *Journal of Building Structures*, Vol. 34, No. Supp1, pp. 66-72, DOI: 1000-6869(2013)S1-0066-07.

Wang, X. (2012). *Experiments on Seismic Behavior of prestressing steel strip constraint strength concrete composite columns*, M.S. Thesis, Xi'an University of Architecture and Technology, Xi'an, Shanxi, China.

Xiong, Z. (2012). *The analysis of the ultimate bearing capacity of concrete filled steel tubular columns high pier*, M.S. Thesis, Zhejiang University of Technology, Hangzhou.

Xu, W., Yu, Q., and Yao, G. (2014). "Effect of preload on the axial capacity of CFST reinforced concrete columns." *Journal of Tsinghua University*, Vol. 54, No. 5, pp. 556-562, DOI: 10.16511/j.cnki.qhdxxb.2014.05.009.

Yao, G. H., Li, Y. J., and Liao, F. (2013). "Behavior of concrete-filled steel tube reinforced concrete columns subjected to axial compression." *Journal of Building Structures*, Vol. 34, No. 5, pp. 114-121, DOI: 10.14006/j.jzjgxb.2013.05.013.

Zhang, W. (2013). *Elastic-plastic Analysis of Steel Tube-reinforced Concrete*, M.S. Thesis, Dalian University of Technology, Dalian.

Zhong, S.T. (2003). *Concrete-Filled Steel Tube Structure*, Tsinghua University Press, Beijing, China.

Zhou, Y., Yu, H., Qian, J., Hu, K., and Qu, G. (2015a). "Moment capacity calculation method on ring beams of joints of concrete filled steel tubular laminated columns." *Journal of Building Structures*, Vol. 36, No. 2, pp. 79-86, DOI: 10.14006/j.jzjgxb.2015.02.010.

Zhou, Y., Yu, H.Y., Qian, J., Qu, G., Hu, K., and Chen, Y. (2015b), "Experimental study on ring beams of joints of concrete filled steel tubular laminated columns." *Journal of Building Structures*, Vol. 36, No. 2, pp. 69-78, DOI: 10.14006/j.jzjgxb.2015.02.009.